Fast subnanometer particle localization by traveling-wave tracking

Lorenzo Busoni, Aurélie Dornier, Jean-Louis Viovy, Jacques Prost, and Giovanni Cappello[a)]
Physico Chimie Curie, Unite Mixte de Recherche (UMR), Centre National de la Recherche/Institut Curie (CNRS/IC) 168, 26 rue d'Ulm, 75248 Paris Cedex 05, France

(Received 22 December 2004; accepted 3 August 2005; published online 20 September 2005)

Traveling-wave tracking (TWT) is a technique for the study of the motion of submicron-sized particles with a very high spatial and temporal resolutions: the particle can be localized with a subnanometer precision at the microsecond time scale. In this technique, a particle is moving through the traveling interference pattern, and measurements of the intensity and phase of the scattered light allow to precisely determine the particles position. In the present paper we describe the experimental setup and its performances. As an example of use of the TWT, we characterize the Brownian motion of a submicron-sized bead in a confined environment. © *2005 American Institute of Physics*. [DOI: 10.1063/1.2043230]

I. INTRODUCTION

An increasing research activity on single-molecule techniques has been emerging over the last ten years. This development is motivated by the necessity to better understand the function and, particularly, the dynamical behavior of enzymes.[1–8]

In order to follow the details of the dynamics of one single protein high spatial and temporal resolutions are required. Recently, we have introduced an optical technique allowing us to track submicron particles with nanometer space resolution and a few microseconds time resolution. This technique was based on the simple idea that if the light intensity used to observe the particle depends on space, then a measure of $I(t)$, the light emitted by the particle as a function of time, provides a direct measure of its position.[9–11] In practice the spatial modulation was obtained by generating a standing wave.[12] Although powerful, it had the drawback of losing sensitivity at each antinode of the standing wave and thus reduced continuous tracking to half a period.

In this manuscript we introduce a technique by which a phase and intensity measurements provide a two-dimensional tracking of the particle over any desired run length. This is achieved by replacing the standing wave by a suitably designed evanescent traveling wave. We call this technique *traveling-wave tracking* (TWT).

In Sec. III B we illustrate the technique by characterizing the Brownian motion of a particle in a confined environment: we report the measurement of the diffusion coefficient of a submicrometer bead free to move close to a surface.

II. EXPERIMENTAL SETUP

Conventional tracking techniques are based on spatially resolved detectors, measuring the light scattered from a relatively small probe, small bead, or fluorescent dye, moving in a uniformly illuminated field or within a spot of laser light. These techniques use charge-coupled device (CCD) cameras or quadrant-photodiode-based detections.

TWT works in the opposite way: the scattered light is recorded by a point detector [avalance photodiode (APD)], with a wide bandwidth (~10 MHz), while the probe moves through a pattern of fringes. The fringes are obtained by interference of two laser beams with slightly different frequencies such that the pattern continuously shifts through the sample at constant speed. As a result, the sample is illuminated by a progressive sinusoidally modulated intensity

$$I(x,t) \propto 1 + \sin(qx + \Omega t),$$

where the fringe periodicity d is $2\pi/q$ and the pattern shifts with a speed $v_f \equiv \Omega/q$. (In our setup $d \approx 200$ nm and $\Omega \approx 4$ MHz.)

Let us imagine a small particle (a 100-nm polystyrene bead) immobile in the microscope: it will be alternately in the light and in the dark with a frequency of Ω. As the bead scatters the light in proportion to the local intensity, it appears to the APD as a blinking dot, and the APD records a signal $I_{\mathrm{APD}} \propto 1 + \sin(\Omega t + \varphi)$, where φ is a phase shift depending on the bead position in the fringes. If the bead moves over a small distance δx from the position x' to $x' + \delta x$, the phase shift will change from φ' to $\varphi' + (2\pi/d)\delta x$, where d is the fringe period. In such a way, any displacement of the bead can be precisely determined, on the condition that we measure the phase shift $\varphi(t)$ as a function of time. In the following we will describe how the *traveling fringes* have been designed and how the phase shift has been measured.

The sinusoidal modulation is obtained by interference of two laser beams, with opposite wave vectors k_x, undergoing total internal reflection at the glass/water interface. In this setup, the fringe periodicity is

$$d = \frac{\lambda_0}{2 n_{\mathrm{glass}} \cos \vartheta}, \tag{1}$$

where λ_0 is the laser wavelength, ϑ is the incidence angle at the glass/water interface, and n_{glass} is the glass refraction index (usually 1.52).

[a)]Electronic mail: Giovanni.Cappello@Curie.fr

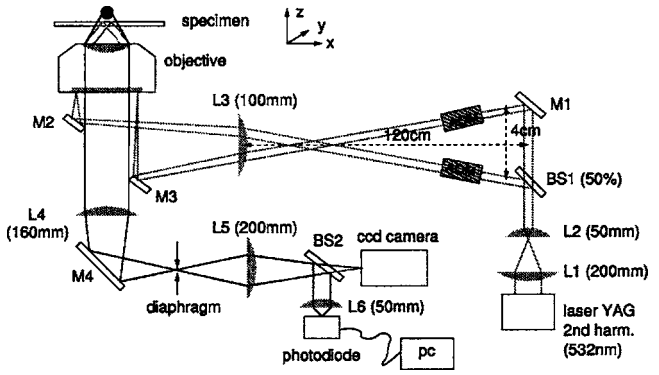

FIG. 1. Schematic of the experimental setup. Traveling-wave tracking configuration through the TIRF objective. The laser beam is compressed by means of a telescope (lenses L_1 and L_2) and split in two beams (beam splitter BS_1) of equal intensity and polarization. The acousto-optic modulators (AOM) shift the frequency of both the laser beams, which are focused (lens L_3) on the diameter of the back focus plane, in order to light the sample with two parallel beams with opposite wave vector k_x. The scattered light is collected by the lenses L_4, L_5, and L_6 and focused on the avalanche photodiode and/or on a CCD camera. M_1, M_2, M_3, and M_4 are mirrors and BS_2 is a 1%–99% beam splitter.

The light is totally reflected at the glass/water interface and the intensity exponentially decreases with a characteristic penetration depth ζ in the direction perpendicular to the interface, where ζ is

$$\zeta = \frac{\lambda_0}{4\pi}(n_{\text{glass}}^2 \sin^2 \vartheta - n_{\text{H}_2\text{O}}^2)^{-1/2}. \tag{2}$$

The optical setup is described in Fig. 1. The laser beam is compressed to a diameter of 1 mm (L_1 and L_2 in Fig. 1) and split by using the beam splitter BS_1: the two beams have similar intensity and polarization and their coherence is preserved. The lens L_3 focuses the beams on two, diametrically opposed, points of the objective back focus plane. In such a way a small region of the specimen (15×15 μm^2) is illuminated by two antiparallel laser beams and an interference pattern is established at the glass/water interface.

In order to obtain a traveling wave, we chose to slightly shift the frequency ω of both the laser beams by $\Delta\omega_1$ and $\Delta\omega_2$, respectively. The frequency difference $\Omega=\Delta\omega_1-\Delta\omega_2$ is typically set to $\Omega/2\pi=4$ MHz in order to obtain a pattern moving much faster than any probe motion: the pattern speed is $v_f=\Omega d/2\pi\approx 1$ m/s. The resulting electric field $\mathbf{E}(x,z;t)$ is the sum of the two beams

$$\begin{cases} \mathbf{E}_1 = \mathbf{E}_0 \exp[i\mathbf{k}\cdot\mathbf{x} - i(\omega+\Delta\omega_1)t]e^{-z/2\zeta}, \\ \mathbf{E}_2 = \mathbf{E}_0 \exp[-i\mathbf{k}\cdot\mathbf{x} - i(\omega+\Delta\omega_2)t]e^{-z/2\zeta}, \end{cases}$$

and the total intensity on the specimen can be written as

$$I(x,z;t) = |\mathbf{E}_1+\mathbf{E}_2|^2 = 2\mathbf{E}_0^2[1+\cos(qx-\Omega t)]e^{-z/\zeta}. \tag{3}$$

The frequencies are modified by using two acousto-optic modulators (AOM-IntraAction, AFM-402A1), whose frequency difference is electronically locked by a dual generator (IntraAction, DFE-404A4).

The light scattered from the probe is collected by the same objective, focused by the lenses L_4, L_5, and L_6 and measured by the avalanche photodiode (Hamamatsu, bandwidth=10 MHz). As explained, the intensity $\mathcal{I}_{\text{APD}}$, measured by the photodiode, is proportional to Eq. (3). The resulting signal is a sinelike modulation at 4 MHz, whose amplitude and phase depend, respectively, on the z and the x positions of the probe. Both, phase and amplitude, can be extracted by comparing the measured intensity to the signal driving the acousto-optic modulators: $f(t)=\cos(\Omega t)$. The two signals $f(t)$ and $\mathcal{I}_{\text{APD}}(t)$ are combined via a homemade lock-in amplifier (See Fig. 2), which measures the complex value

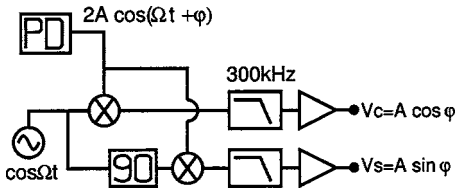

FIG. 2. Schematic of the demodulator (lock-in amplifier). The photodiode (PD) signal is amplified (A1) and split into two channels (split). Channel one is multiplied (⊗) by the reference signal $\cos(\Omega t)$ and channel two by the reference signal shifted (90) by $\pi/2$. The two low-pass filters (300 kHz) remove the higher harmonics and amplify the signals $V_C=\cos(qx)e^{-z/\zeta}$ and $V_S=\sin(qx)e^{-z/\zeta}$. A1 is a Minicircuits ZHL-6A, mixers (⊗) are Minicircuits ZAD-6, 90 shifter (90) is a homemade LC filter, lowpass filters are homemade fifth-order LC Butterworth filters.

$$V(t) = \langle \mathcal{I}_{\text{APD}}(t')|e^{-i\Omega t'}\rangle = V_C(t) + iV_S(t). \tag{4}$$

From $V_C(t)$ and $V_S(t)$, simultaneously recorded with a bandwidth of 300 kHz and a sample rate of 625 ksample/s, we can finally calculate the two coordinates $x(t)$ and $z(t)$,

$$\begin{cases} x(t) = d/2\pi \arg V(t), \\ z(t) - z_0 = -\zeta \ln|V(t)|. \end{cases} \tag{5}$$

Note that the absolute value of the intensity is unknown and we can only measure intensity variations. This implies that we do not know the absolute z position of the probe, but we can only measure relative motions $z(t)-z_0$.

Experiments are carried out using an Olympus 60X total internal reflection fluorescence (TIRF) objective (numerical aperture 1.45) and a CCD camera. The laser source is a second-harmonic yttrium aluminum garnet (YAG) (Coherent Verdi), with a wavelength $\lambda_0=532$ nm and a longitudinal coherence length of several meters. Its power is typically set to 500 mW.

III. RESULTS

A. Setup performances

The resolution and the performances of this setup have been characterized using a piezoelectric stage, moving a bead stuck to the coverglass. The piezoelectric stage moves by 20-nm steps (the resolution of the stage is ±5 nm) every 200 ms. The motion is reflected by a phase shift. Figure 3 shows how the phase $\varphi(t)$ evolves as a function of the time. We observe the well-defined 20-nm steps with sharp edges. The phase (right axis on the plot) changes linearly with the position (left axis). This allows us to calibrate the instrument: within the piezoelectric stage accuracy, the fringe period is 197±2 nm. By using Eqs. (1) and (2) the penetration depth

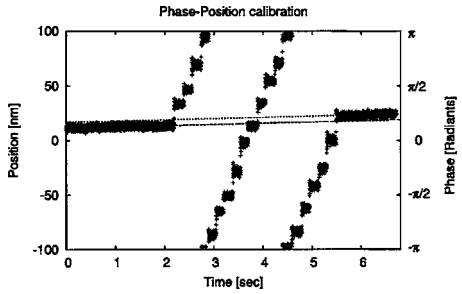

FIG. 3. A single colloid (diameter 200 nm) is fixed on the coverglass, while the sample holder is moved in 20-nm steps by means of a calibrated piezoelectric stage.

can be estimated: $\zeta = 230 \pm 90$ nm. The uncertainty associated to this estimation is large: we will see in Sec. III B another way to calibrate this parameter.

Figure 3 also reveals a constant positive drift. It gives an indication of the long-time stability of our setup, which is roughly 1 nm/s. This stability is not a limiting factor for extremely rapid events, such as molecular motor motion at high ATP concentration, whose speed can reach 2 μm/s. Conversely, it could become critical for observing slowly moving objects. We also notice in Fig. 3 that the phase is undetermined by a factor of 2π: this is not a major problem for our experiments because the observed object never covers more than few tens of nanometers within our sampling interval δt. This puts an upper limit of $v = d/\delta t$ on observable velocities without any ambiguity. In practice this is not a severe limitation; for instance, a globular protein ($\sim$5 nm in diameter) in water has a diffusion coefficient of 84 nm$^2/\mu$s: it diffuses only $\sim$16 nm during the sampling interval of 16 μs. This value is small compared to the fringe period $d = 200$ nm.

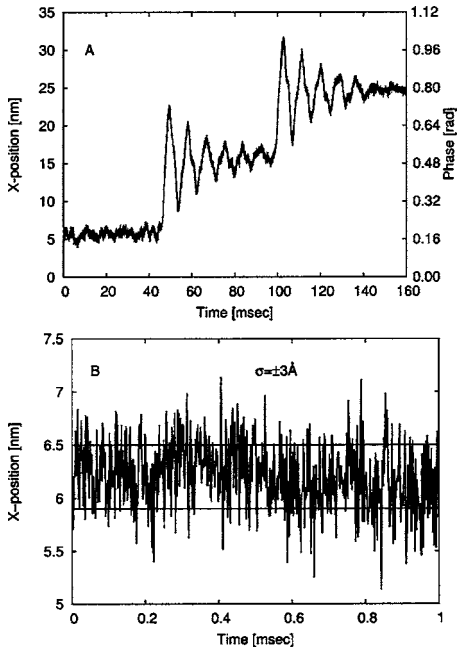

FIG. 4. (A) A single colloid (diameter 200 nm) is fixed on the coverglass, while the sample holder is moved in 10-nm steps by means of a calibrated piezoelectric stage. (B) the residual shot noise limits the resolution to 3-Å rms.

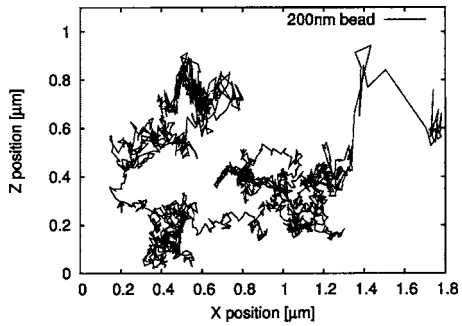

FIG. 5. 2D tracking of a 200 nm bead diffusing close to the sample coverslip ($z=0$). Directions x and z are parallel and perpendicular to the surface, respectively. While the trajectory is acquired with full bandwidth (625 ksample/s) in order to improve the visibility of the track only one point out of one hundred has been plotted.

Figure 4(a) shows two 10-nm steps in a row, acquired with full bandwidth: the 10-nm displacement are easily observed and the internal structure of the step can be characterized with nanometer precision. The oscillatory motion after the step is due to the inertial behavior of the piezoelectric stage: without any feedback loop, it oscillates with exponentially damped amplitude after steplike impulses. The intrinsic noise of the experimental setup can be measured by analyzing the parts of the curve where the oscillations are completely damped [see Fig. 4(b)]. The plot shows that the intrinsic noise is 3-Å rms; this noise, which is *white* and totally uncorrelated, is due the residual shot noise.

If we compare the TWT with a *quadrant photodiode* detection, we notice that the TWT improves the space resolution up to a factor of 10 with the same bandwidth. This improvement is due to the lock-in detection that filters out all the low-frequency noises, including electronic (amplification and detection instabilities) and optical instabilities (laser intensity fluctuations and mechanical instabilities). This is confirmed by the fact that also in our setup the resolution deteriorates by a factor of 30 in the absence of the lock-in detection and with the full bandwidth (data not shown).

B. Wall limited Brownian motion

In order to illustrate this technique, the TWT has been used to characterize the Brownian motion of a submicrometer particle diffusing close to a wall. The two-dimensional motion (parallel and perpendicular to the surface) has been

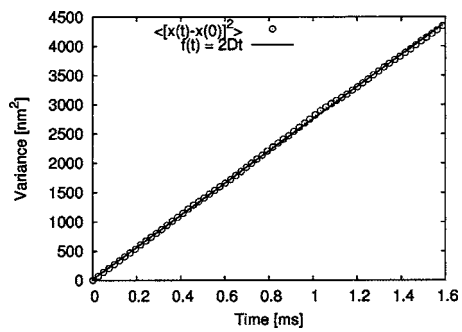

FIG. 6. Mean square of the bead fluctuation as a function of time: $\langle \Delta x^2 \rangle = \langle [x(t) - x(0)]^2 \rangle$, for a 200-nm bead. The initial distance between the bead and the surface is 170 nm, which corresponds to $z/r = 1.7$ in Fig. 7.

TABLE I. Theoretical and measured values of the diffusion coefficients for 200, 300, and 500 nm beads, respectively.

Bead diameter (nm)	Theoretical D_0 ($nm^2/\mu s$)	Measured D_0 ($nm^2/\mu s$)
210±3	2.02±.03	1.87±.04
314±5	1.35±.02	1.21±.04
517±11	0.82±.02	0.80±.05

recorded for many seconds with full bandwidth, as shown in Fig. 5 (to improve the visibility only every hundredth point have been plotted).

We have measured the motion of spherical polystyrene beads of diameter 0.2, 0.3, and 0.5 μm. The diffusion coefficient can be measured from the fluctuations of the bead as a function of time,

$$\overline{\Delta x(t)^2} = \langle [x(t) - x(0)]^2 \rangle = 2D_0 t,$$

$$\overline{\Delta z(t)^2} = \langle [z(t) - z(0)]^2 \rangle = 2D_0 t. \tag{6}$$

For a spherical particle of radius R, in a Newtonian fluid far from any boundary, the diffusion coefficient D_0 is given by the Stokes-Einstein equation[13]

$$D_0 = (k_B T)/(6\pi\eta R), \tag{7}$$

where η is the viscosity of the fluid. Brenner[14] demonstrated that the diffusion coefficient is strongly affected by a confined environment and decreases in the vicinity of a wall. Therefore, the diffusion coefficient is a function of the distance between the bead and the surface.[15,16] In addition, it also depends on the direction of motion and two diffusion coefficients should be defined: $D_x(z)$ and $D_z(z)$ for the motion parallel and perpendicular to the surface, respectively. Those diffusion coefficients are different ($D_x \neq D_z$) and they should be calculated for each position $\bar{z}$ above the surface. In order to take in account this effect, the data have been analyzed with a time window of 1.6 ms, which corresponds to 1000 acquired points; within each window we compute $\overline{\Delta x(t)^2}, \overline{\Delta z(t)^2}$, and the mean position above the surface $\bar{z}$. Figure 6 shows the mean square of the fluctuations $\overline{\Delta x(t)^2}$ for a 200-nm bead diffusing at ~170 nm from the coverslip. The average has been done on about 1000 realizations, and the time over which Eq. (6) holds is restricted to windows such $\sqrt{\overline{\Delta x(t)^2}} \ll \bar{z}$. The straight line is the best fit of $D_x^{200}(50\text{ nm})$ according to Eq. (6).

The diffusion coefficients D_x and D_z have been measured for different altitudes $\bar{z}$ and for beads of 200, 300, and 500 nm of diameter. The values of D_x are in good agreement with the analytical equations proposed by Brenner for the lateral and perpendicular corrections,

$$D_x = D_0 \left[1 - \frac{9}{16}(r/z) + \frac{1}{8}(r/z)^3 - \frac{45}{256}(r/z)^4 - \frac{1}{16}(r/z)^5 \right], \tag{8}$$

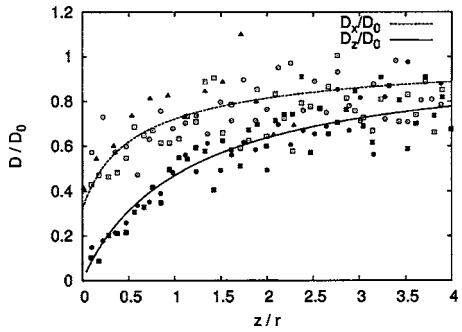

FIG. 7. Parallel (D_x; empty marks) and perpendicular (D_z; filled marks) diffusion coefficient as a function of the bead-surface distance parameter z/r (distance/bead radius). The diffusion coefficient is normalized to the diffusion far from the surface D_0; it has been measured for beads of 200 (□), 300 (○), and 500 (△) nm.

$$D_z = \frac{3}{4\sinh\alpha} D_0 \left\{ \sum_{n=1}^{\infty} \frac{n(n+1)}{(2n-1)(2n+3)} \times \left[\frac{2\sinh(2n+1)\alpha + (2n+1)\sinh 2\alpha}{4\sinh^2(n+1/2)\alpha - (2n+1)^2 \sinh^2\alpha} - 1 \right] \right\}^{-1}$$

with

$$\alpha = \cosh^{-1}(z/r). \tag{9}$$

The experimental data are fitted to Eq. (8) with two adjustable parameters: D_0 and z_0. D_0 is the diffusion coefficient $D_x(\infty)$ far from the wall and z_0 is an arbitrary offset due to the relative measurement of z, discussed in Sec. II. The results are summarized in Table I: for each diameter the theoretical diffusion coefficient calculated from Eq. (7) is compared to the experimental asymptotical coefficient D_0 supplied by fitting the data to Eq. (8).

By comparing the perpendicular diffusion coefficient D_z to Eq. (9) and keeping the same D_0 and z_0, we can independently calibrate the penetration depth ζ of the evanescent wave. Experimentally we find $\zeta \sim 215$ nm, which is consistent with the value estimated in Sec. III A.

All the $D_x(z)$ and $D_z(z)$ are plotted simultaneously (Fig. 7) as a function of the position parameter z/r (sphere-surface distance/bead radius). For each bead size, the diffusion coefficient is normalized to their bulk values D_0. The continuous lines show normalized diffusion coefficients according to Eqs. (8) and (9), which are in good agreement with the experimental data.

IV. CONCLUSION

We have introduced a simple, versatile, and powerful technique for tracking submicrometer objects: the *traveling-wave tracking*. The TWT allows us to follow the particle position along two directions with a lateral resolution of 3 Å and a time resolution in the microsecond range. The extension to three dimensions is in principle straightforward. We probed this technique by measuring the Brownian motion of a polystyrene bead in a confined environment.

Considering the time-space resolution achieved by the TWT, we expect this technique to be a useful tool for investigating biological objects moving on the subnanometer scale.

We warmly thank Professor M. Carlà for his assistance in the development of the electronics, and Professor A. Ott for the fruitful discussions. This work was supported by the grants from the *E. U.* (BIOMACH project).

[1]K. Svoboda, C. F. Schmidt, B. J. Schnapp, and S. M. Block, Nature (London) **365**, 721 (1993).
[2]E.-L. Florin, V. T. Moy, and H. E. Gaub, Science **264**, 415 (1994).
[3]R. Merkel, P. Nassoy, A. Leung, K. Ritchie, and E. Evans, Nature (London) **397**, 50 (1999).
[4]J. T. Finer, R. M. Simmons, and J. A. Spudich, Nature (London) **368**, 113 (1994).
[5]K. Visscher, M. J. Schnitzer, and S. M. Block, Nature (London) **400**, 184 (1999).
[6]M. Nishiyama, E. Muto, Y. Inoue, T. Yanagida, and H. Higuchi, Nat. Cell Biol. **3**, 425 (2001).
[7]C. Veigel, J. Molloy, S. Schmitz, and J. Kendrick-Jones, Nat. Cell Biol. **5**, 980 (2003).
[8]A. Yildiz, M. Tomishige, R. D. Vale, and P. R. Selvin, Science **303**, 676 (2004).
[9]G. Cappello, M. Badoual, L. Busoni, A. Ott, and J. Prost, Phys. Rev. E **68**, 021907 (2003).
[10]A. Dornier, L. Busoni, K. Zeldovich, B. Guirao, G. Robin, G. Cappello, and J. Prost, J. Biol. Phys. Chem. **4**, 74 (2004).
[11]M. Badoual, G. Cappello, K. Zeldovich, and J. Prost, Eur. Phys. J. E (in press).
[12]K. B. Migler, H. Hervet, and L. Leger, Phys. Rev. Lett. **70**, 287 (1993).
[13]A. Einstein, Ann. Phys. **17**, 549 (1905).
[14]H. Brenner, Chem. Eng. Sci. **16**, 242 (1961).
[15]L. P. Faucheux and A. J. Libchabert, Phys. Rev. E **49**, 5158 (1994).
[16]A. Pralle, E.-L. Florin, E. Stelzer, and J. Hörber, Appl. Phys. A: Mater. Sci. Process. **66**, S71 (1998).